Acta Metallurgica Sinica (English Letters) (2020) 33:551–560
https://doi.org/10.1007/s40195-019-00968-2

Effect of Sleeve Plunge Depth on Interface/Mechanical Characteristics in Refill Friction Stir Spot Welded Joint

Guang-Da Sun[1,2] · Li Zhou[1,2] · Ren-Xiao Zhang[2] · Ling-Yun Luo[2] · Hao Xu[2] · Hong-Yun Zhao[2] · Ning Guo[1,2] · Di Zhang[3]

Received: 15 July 2019 / Revised: 27 August 2019 / Published online: 2 December 2019

Abstract
Refill friction stir spot welding was employed to produce 6061-T6 aluminum alloy joints with different sleeve plunge depths. The interface characteristics of joint-line remnant and hook are investigated by optical and scanning electron microscopy. The joint-line remnant consists of primary bonding region and secondary bonding region, and two types of hook can be identified as downward hook and upward hook. Tensile shear results demonstrate that joint-line remnant and hook make interaction effects on tensile shear properties. The optimal joint is achieved when sleeve plunge depth was 2.0 mm with the corresponding failure load of 8673.4 N. Three different types of fracture mode are exhibited in joints produced at different sleeve plunge depths, which are closely related with the morphology of interface characteristics.

Keywords Refill friction stir spot welding · Interface characteristics · Mechanical properties · Fracture behavior

1 Introduction

With the deterioration of environment and energy depletion, lightweight is a major trend of automotive industry to reduce fuel consumption and CO_2 emission [1, 2]. Aluminum alloys, as common lightweight materials, are widely applied to replace steel in automotive and aerospace industry [3, 4]. Refill friction stir spot welding (RFSSW), derived from traditional friction stir spot welding, can produce keyhole-free joints with higher static strength and fatigue strength. Thus, RFSSW is deemed to be a promising technology for joining aluminum alloy in automotive and aerospace industry [5, 6].

The tool assembly employed in RFSSW is composed of clamp ring, sleeve and pin [7]. The function of clamping ring is to statically hold plates against the anvil, and the sleeve and pin move up and down independently to achieve material refilling. The process of RFSSW is divided into four stages [8, 9], as shown in Fig. 1. In pre-friction stage, the tool is positioned with a given pressure onto the to-be-welded plates with the rotating sleeve and pin. In penetration stage, the rotating sleeve plunges downwards to a desired depth with given velocity. Simultaneously, the pin moves away from the plate, creating a space for the plasticized material. Then the sleeve moves upward and the pin moves downward in refill stage to push the plastic material into space created by the sleeve. Finally, the tool is withdrawn leaving a keyhole-free weld in pull-out stage [10].

Previous studies have pointed that tensile shear properties of RFSSWed joint were significantly affected by the interface characteristics of joint-line remnant and hook [11–13]. Tier et al. [7, 14] indicated that the morphology of joint-line remnant exerts an important effect on the mechanical performance. Larger joint-line remnant length was presented in the joint with rectangular stir zone morphology, which results in better tensile shear properties. Besides, the hook is considered to be a crucial geometry feature in FSSW welds as Badarinarayan et al. [15] reported. Cao et al. [16] revealed that upward hook could reduce the effective top sheet thickness in RFSSWed joint. It was demonstrated that higher hook height tends to make lower tensile shear properties. Rosendo et al. [17] showed that hook will diminishes the integrity of joint

Available online at http://link.springer.com/journal/40195

✉ Li Zhou
zhouli@hitwh.edu.cn

1 State Key Laboratory of Advanced Welding and Joining, Harbin Institute of Technology, Harbin 150001, China

2 Shandong Provincial Key Laboratory of Special Welding Technology, Harbin Institute of Technology at Weihai, Weihai 264209, China

3 State Key Laboratory of Advanced Metals and Materials, University of Science and Technology Beijing, Beijing 100083, China

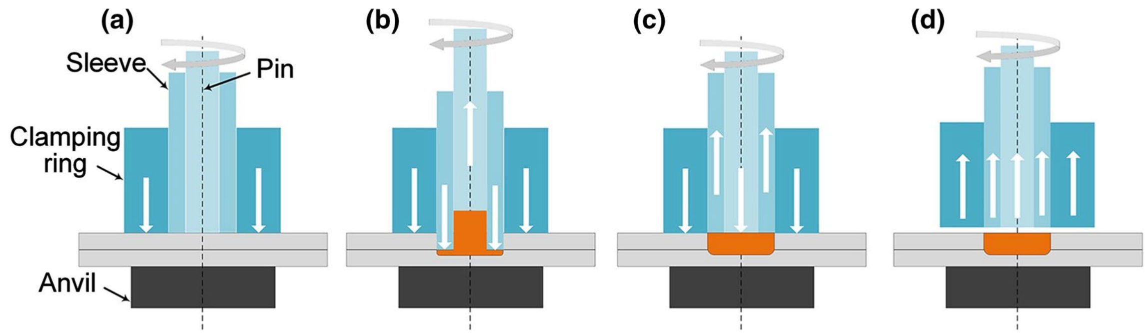

Fig. 1 Schematic illustration of RFSSW processes: **a** pre-friction stage, **b** penetration stage, **c** refill stage, **d** pull-out stage

and boost the crack nucleation, thereby deteriorating the tensile shear properties. Zhao et al. [11, 12] indicated that sleeve plunge depth significantly affects joint properties and associated tensile shear properties to the hook geometry and the existence of weld defects including annular groove and voids.

Literature determines that for RFSSW, the interface characteristics have an important influence on the mechanical properties of joint, and many researches were focused on the effects of joint-line remnant or hook. However, studies about comprehensive effects of joint-line remnant and hook on mechanical properties of joint are deficient. Consequently, the present study is aimed to understand the relationship between sleeve plunge depth, interface characteristics and mechanical properties in 6061-T6 aluminum alloy RFSSWed joint.

2 Experimental

RFSSW was conducted on rolled 6061-T6 aluminum alloy sheets with the dimension of 80 mm × 30 mm × 2 mm. The chemical composition and mechanical properties of base material are presented in Table 1. All sheets were thoroughly milled and then cleaned with acetone to remove oxidation layers and oil stain prior to welding. The welding was performed by an RFSSW machine developed in-house. The overlap area of two sheets is 30 mm × 30 mm with the welding spot in the center. The RFSSW tool system is composed of a 18-mm-diameter champing ring, a 9-mm-diameter sleeve and a 5.3-mm-diameter pin. During welding, tool rotation speed, sleeve plunge speed and pre-friction time were kept constant at 1500 rpm, 1 mm/s and 2 s for all joints, while various sleeve plunge depths of 1.75, 2.0, 2.25 and 2.5 mm were employed.

After welding, metallographic specimens were cut by an electric discharge machine (EDM), polished with 1 μm diamond paste and etched by Keller reagent for 150 s. Then, as-prepared samples were observed by an optical microscope (OM-Olympus GX51) and a scanning electron microscope (SEM-TESCAN VEGAII) for examination of macro-/microstructure. Vickers hardness was measured every 0.5 mm at mid-thickness of upper sheet using a MICRO-586 microhardness tester with a load of 200 g for 10 s. Tensile shear test was performed on INSTRON-1186 universal machine at crosshead displacement rate of 1 mm/min. Shims with same material and thickness were applied to prevent the load axis deviating during test. To ensure the reliability of testing results, three samples for each parameter were employed. Afterward, SEM was utilized to analyze fracture surface morphologies of the joints.

3 Results and Discussion

3.1 Macro-/Microstructure Characteristic

Keyhole-free joint without obvious defect is obtained, as shown in Fig. 2a. The welded spot can be divided into three zones as follows: heat-affected zone (HAZ), thermo-mechanically affected zone (TMAZ) and stir zone (SZ). Two interface characteristics of joint-line remnant and hook can be observed in joint cross section (Fig. 2b).

3.1.1 Interface Characteristic

The joint-line remnant is interpreted as the remnant oxide film originating from the faying surface [18]. It is considered to be a region which can reflect the metallurgical bonding between two sheets, and can be divided into two parts:

Table 1 Chemical composition and mechanical properties of 6061-T6 aluminum alloy

Chemical compositions (wt%)									Mechanical properties	
Mg	Si	Fe	Ti	Cu	Cr	Zn	Mn	Al	Tensile strength	Microhardness
0.9	0.6	0.7	0.5	0.3	0.26	0.25	0.15	Bal.	310 MPa	95 HV

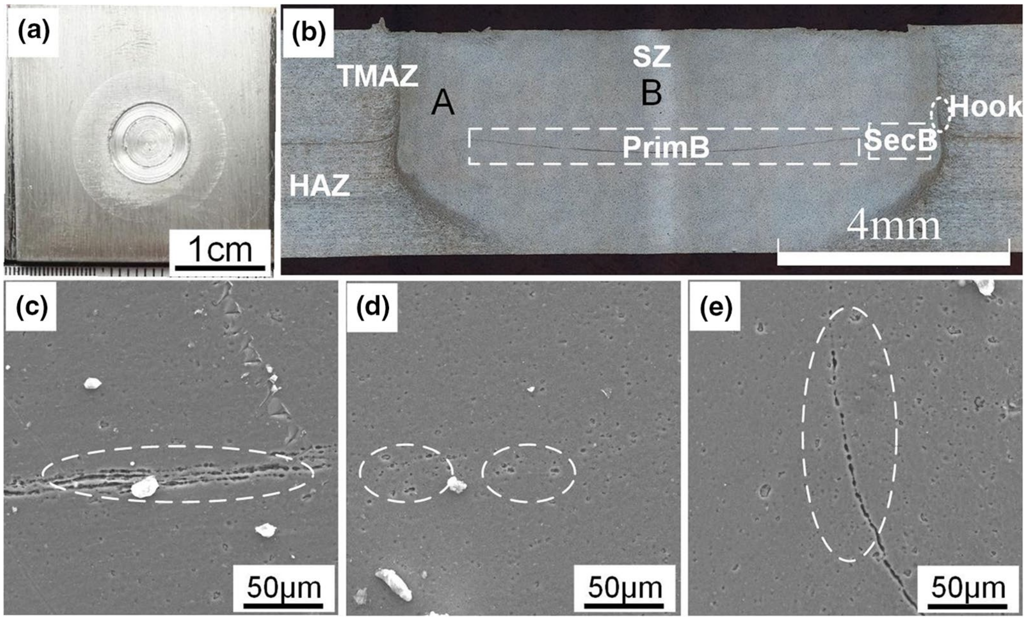

Fig. 2 Joint obtained at sleeve plunge depth of 2.5 mm: **a** surface appearance, **b** cross section, **c** PrimB, **d** SecB, **e** hook

primary bonding region (PrimB) where plenty of remnant oxide films distribute continuously and secondary bonding region (SecB) where few remnant oxide films exist [14]. The PrimB is located at the joint center which is subjected to relatively low strain and strain rate; therefore, the interface cannot be broken completely with many oxide films remained [13]. As illustrated in Fig. 3, the length of PrimB decreases first and then remains stable eventually with plunge depth. The length of PrimB will surely affect the tensile shear properties of joints. The SecB is located at margin of SZ, which experiences the most complex material flow in RFSSW. The initial interface is completely broken, as shown in Fig. 2d; thus, the interface at SecB is not pronounced with only few remnant oxide films existing in the joint. Tier et al. [14] suggested that SecB will be eventually suppressed depending on the welding parameters. In the present study, no SecB is observed at plunge depth of 1.75 mm (Fig. 3a). Only when plunge depth is equal to or greater than 2.0 mm, PrimB and SecB will both appear in the joint. The reason is that the material flow around the interface is mild when plunge depth is less than sheet thickness. Interface in the joint cannot be broken and SecB cannot be found with plunge depth of 1.75 mm. Furthermore, it is found that the SecB performs better than PrimB in tensile shear test which will be proved in below. That is to say, the joint with shorter PrimB and longer SecB tends to possess better tensile shear properties.

Hook is a characteristic feature as a result of the bending sheet interface [19]. Material flow behavior in the TMAZ can be reflected by the hook morphology. Two types of hook can be identified as downward hook and upward hook, whose formation is greatly affected by the plunge depth (Fig. 4). Shen et al. [18] have reported that

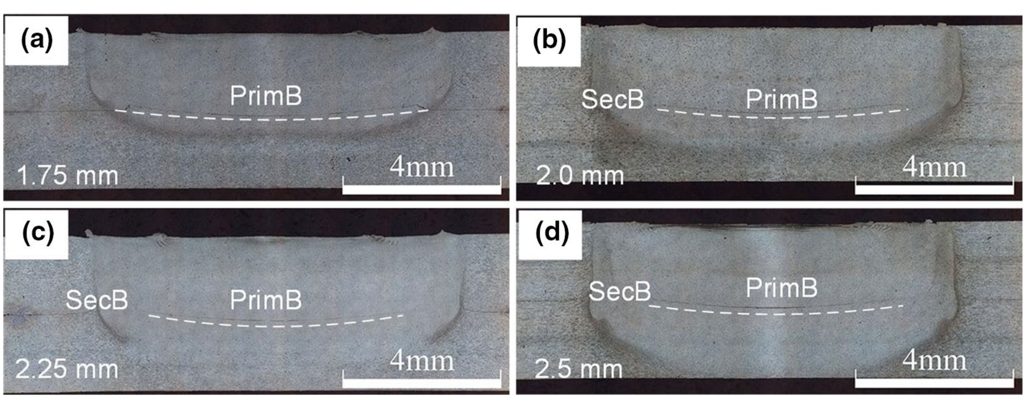

Fig. 3 Interface characteristics of joints with different sleeve plunge depths: **a** 1.75 mm, **b** 2.0 mm, **c** 2.25 mm, **d** 2.5 mm

the initial interface will become deformed during penetration stage even when the plunge depth is less than upper sheet thickness. However, the weak material flow near the interface owing to the fact that the sleeve has not reached the lower plate cannot form evident hook at SZ margin at sleeve depth of 1.75 mm. In fact, hook was formed during the plunging stage; however, it was shrunk down by the material flow during the refilling stage. Increasing plunge depth to 2 mm which is equal to the plate thickness, the hook exhibits downward curved profiles as Cao et al. [16] reported. This difference may arise from the material flow during penetration stage and refill stage. In plunge stage, the material beneath sleeve was extruded into SZ center due to the downward movement of sleeve and upward movement of pin. Meanwhile, the interface underneath the sleeve bends downward, while the interface underneath the pin moves upward because of the material flow. In refill stage, as the material is refilled back by the movement of sleeve and pin, the interface located in the middle was pushed downward by pin. Nevertheless, the bent interface at SZ margin cannot be eliminated by the sluggish material flow thereby forming downward hook. When plunge depth is greater than plate thickness, the hook morphology changes upward, as shown in Fig. 4c, d. Yue et al. [20] demonstrated that the penetration of tool into the lower sheet results in the upward bending interface. As we all know, plastic material flows downwards along the thread and is released at the joint bottom during the welding process, resulting in the formation the material accumulated zone. Thus, the material relative far away from the joint

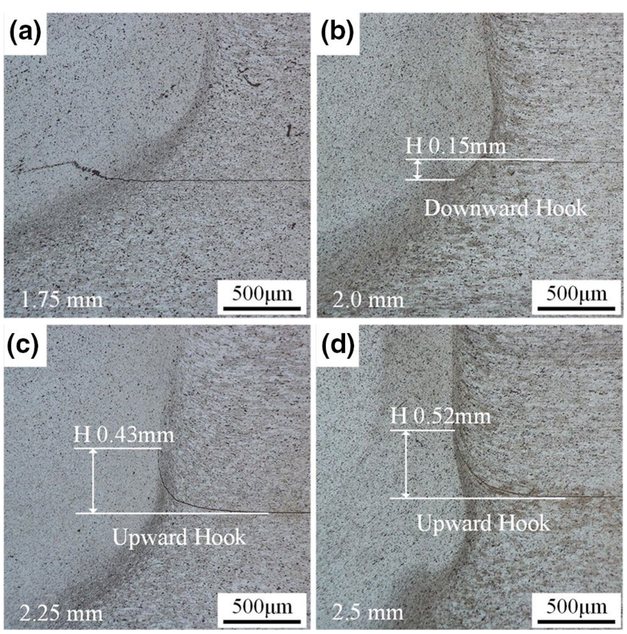

Fig. 4 Hook morphologies of joints with different sleeve plunge depths: **a**1.75 mm, **b** 2.0 mm, **c** 2.25 mm, **d** 2.5 mm

is forced to bend upwards and forms the upward hook. The height of hook (H) represents vertical distance from hook tip to primary interface, which is an important geometric characteristic [21]. H increases with plunge depth owing to the increment of plasticized material volume and heat input. Hook will reduce effective sheet thickness and induce stress concentration during tensile shear test, and the hook morphology will influence the crack path [5]. Thus, hook along with the joint-line remnant plays a great role in tensile shear properties and causes different fracture modes. Generally, the tensile shear properties decreased monotonically with increasing the hook height as Cao et al. indicated [22].

3.1.2 Microstructure Characteristic

Figure 5 presents the microstructure of various zones in typical weld obtained with plunge depth of 2.25 mm. Elongated grains along the rolling direction are presented in the BM, as shown in Fig. 5a. The HAZ only experiences thermal cycle during welding. The temperature of thermal cycle is relatively low and its time is short. So, the changes of microstructure in the HAZ (Fig. 5b) are not obvious compared with BM. In the TMAZ, the grains bent upward without the occurrence of recrystallization owing to moderate temperature and deformation strain [23]. The SZ experiences dynamic recrystallization owing to severe plastic deformation and high temperature [24]. Fine equiaxed grains are formed in this zone. Additionally, grain size and morphology are rather different between edge and center of SZ (regions A and B marked in Fig. 2b). Finer grains are obtained in region A, which can be ascribed to different strain rates in two regions [13]. Region A is located at sleeve stir zone which experiences the most severe plastic deformation, while region B is located at weld center with lowest strain rate [25]. Besides, the grains in region A present a certain direction which coincide with that of material flow in refill stage.

Figure 6a and b shows grains of TMAZ at different plunge depths. The upward bending degree of grains increases with plunge depth. The reason is similar with that of increasing height of hook. Figure 6c and d shows the grains of SZ at different plunge depths. The grain size of SZ changes slightly with increasing sleeve plunge depth. Su et al. [26] proposed that the plunge depth of tool makes an important role in heat production in FSSW, and the same conclusion can be summarized in RFSSW. That is, the total heat input (Q) increases with plunge depth. In addition, as plunge depth increases, the volume of SZ becomes larger accordingly. The heat input (Q) per volume is almost not changed, which exerts little influence on the grain size.

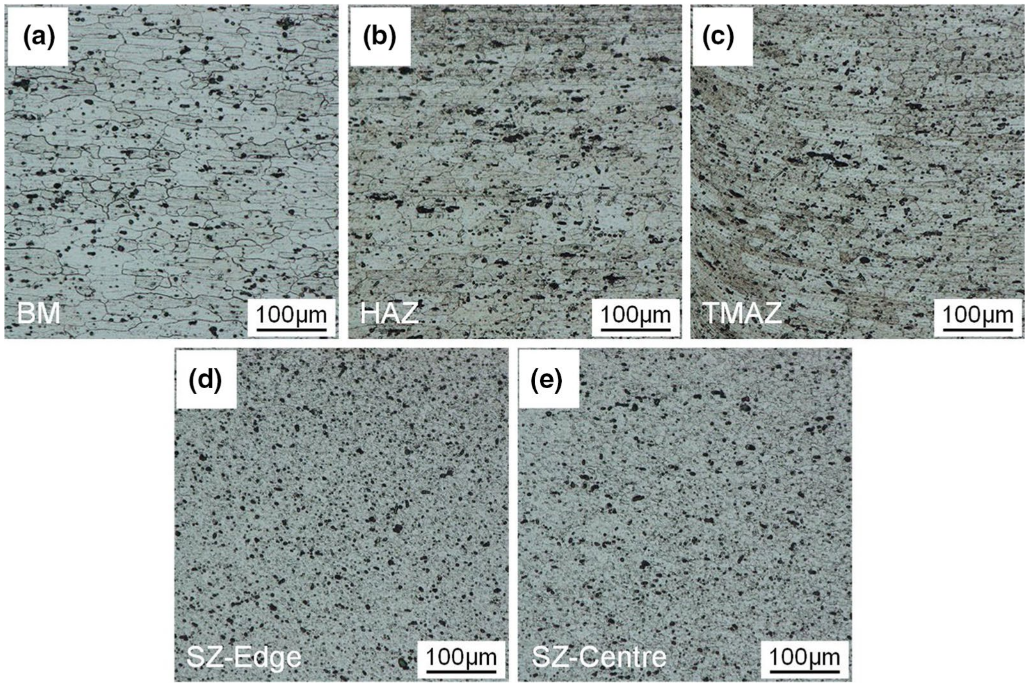

Fig. 5 Grain structures in different microstructural zones of typical joint: **a** BM, **b** HAZ, **c** TMAZ, **d** SZ edge, **e** SZ center

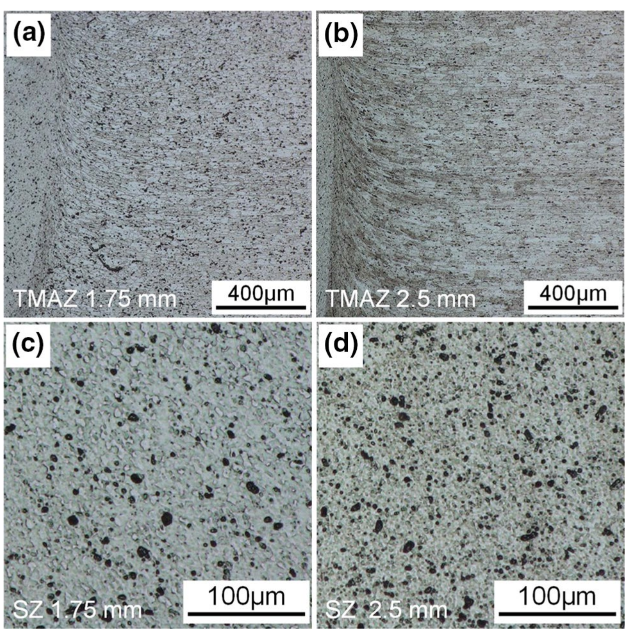

Fig. 6 Grain structures in joint with different sleeve plunge depths: **a** TMAZ formed at 1.75 mm **b** TMAZ formed at 2.5 mm **c** SZ formed at 1.75, **d** SZ formed at 2.5 mm

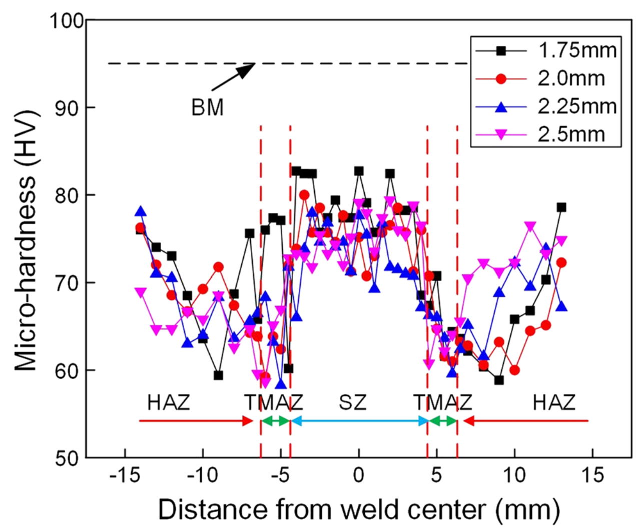

Fig. 7 Hardness distribution at mid-thickness of upper sheet of the joint under different sleeve plunge depths

3.2 Mechanical Properties

3.2.1 Hardness Distribution

The hardness distribution under different plunge depths is illustrated in Fig. 7. Overall, the hardness of the welds was softened compared to the base material (about 95 HV) due to the coarsening and dissolution of precipitation [16], and the hardness distribution presents "W" shape which is generally symmetrical with the weld center. In the softened zone, refined grains formed in the process of dynamic recrystallization leads to the higher hardness in the SZ [27]. Then, the hardness decreases rapidly from TMAZ toward HAZ. The reason is that the effect of working hardening dramatically weakens with the increase in distance from weld center and the thermal cycle plays a leading role in hardness which causes the growth of precipitates and grains [28]. Moreover, the hardness of SZ decreases obviously with the increase in plunge depth. Zhao et al. [12] believed that relative low heat input in small plunge depth will lead to smaller grain size and higher hardness. However, the fact in this investigation is that the grain size changes slightly with plunge depth. A possible explanation for the decreased hardness is that the long welding time will lead to coarser precipitates in SZ at large sleeve plunge [29].

3.2.2 Tensile Shear Properties

Figure 8 presents the tensile shear fracture load (TSFL) of joints at various plunge depths. TSFL firstly increases with sleeve plunge from 1.75 to 2.0 mm and then decreases at 2.25 mm. The maximum TFSL of 8763.4 N is attained at plunge depth of 2.0 mm, while the minimum TFSL is measured to be 5598.7 N with 1.75 mm plunge depth which is less 0.25 mm than sheet thickness of 2 mm. Cao et al. [16] found the similar relationship between plunge depth and TSFL. It is evident that temperature and pressure at interface are relative low when plunge depth is less than upper sheet thickness, longer PrimB without SecB is presented at

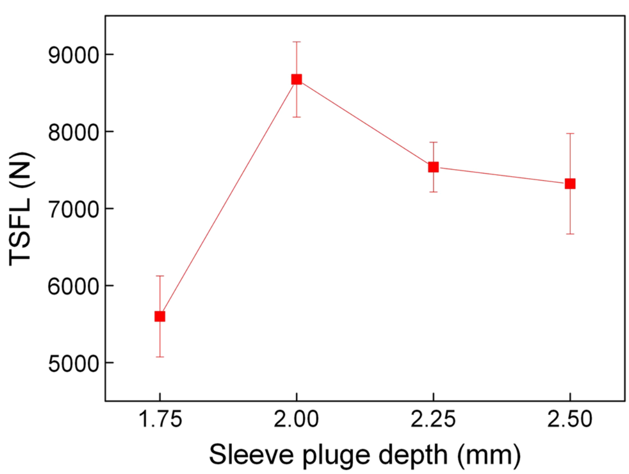

Fig. 8 Correlation of sleeve plunge depth with TFSL

such plunge depth, which results in low interface bonding strength. Increasing plunge depth to 2 mm, the appearance of SecB and shorten of PrimB significantly increase the bonding strength, which indicates that the SecB performs much better than PrimB in the tensile shear test. Furthermore, the occurrence of TFSL decreased at plunge depth more than 2 mm can be attributed to the longer welding time which softens the joint and the higher hook which reduces the effective top sheet thickness.

3.3 Fracture Behavior

Three typical fracture behaviors can be observed: shear fracture, plug fracture and tensile shear fracture [30, 31]. The tensile shear sample presents shear fracture with the lowest TFSL when plunge depth is 1.75 mm. In this condition, a weak material flow occurs at the interface causing a bad bonding between two sheets. When joint is subjected to the load, crack easily initiates and propagates along PrimB to cause the separation of two sheets, as shown in Fig. 9. SEM images as shown in Fig. 10 are taken from the fracture surface to investigate the fracture micromorphology. The fracture surface mainly includes three types of micromorphology, as shown in Fig. 10a. Region B is located at weld periphery. Little influenced by the thermal cycle and stir action, this region presents very low bonding strength. Therefore, smooth tear ridges can be observed in this region. Regions C and D are both located at PrimB with different micromorphologies presented in Fig. 10c,d. Region C is characterized by few tear ridges, substantial micro-dimples and polyhedron morphology, while region D presents the smooth surface. Since region C is closer to sleeve and experiences higher stress and stress rate than region D, the bonding strength of region C is more excellent than that of region D.

Plug fracture is observed in the joint produced at 2 mm plunge depth. The nugget separates from the sheets after tensile shear test and only partially connects with lower sheet. According to the research of Rosendo et al. [17], the stress distribution under tensile shear loading is shown as Fig. 11b. The crack initiates at hook tip for tensile stress concentration and propagates downward along with the downward hook in tensile shear test [5]. In the other side, the downward hook

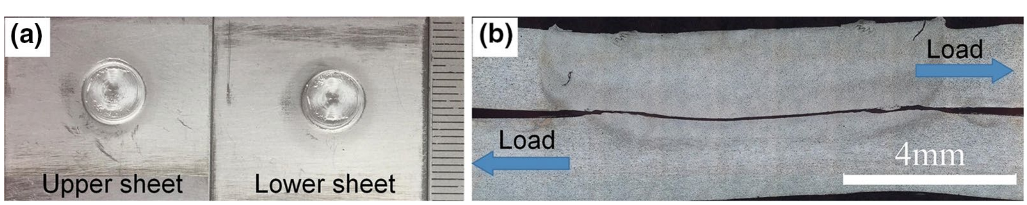

Fig. 9 OM images for shear fracture: **a** macroscopic fracture, **b** cross section

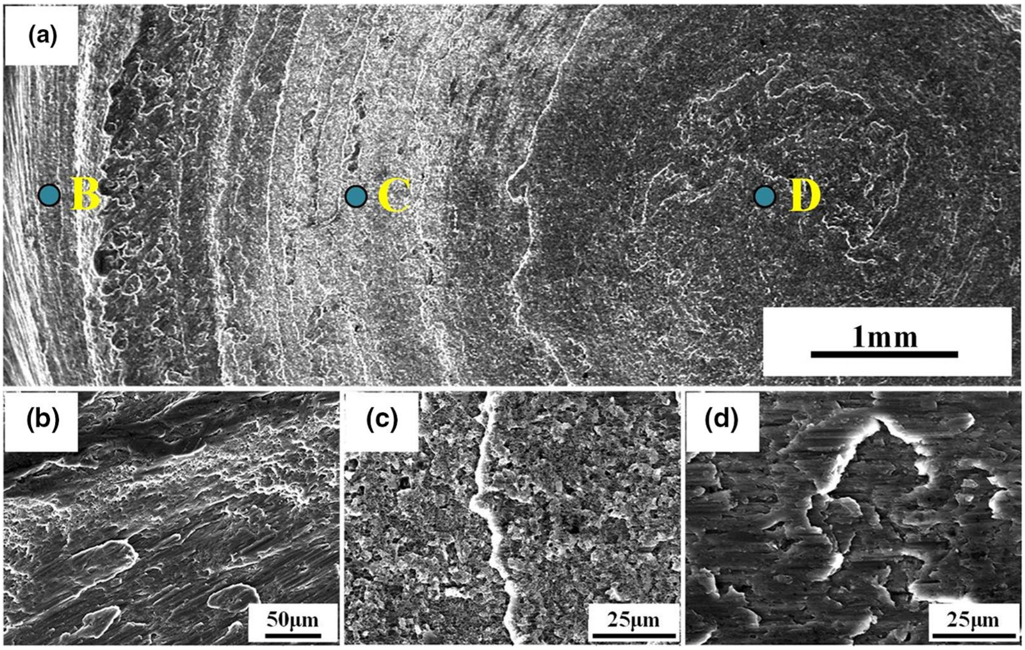

Fig. 10 SEM images of: **a** shear fracture surface, **b–d** magnified views of the regions B–D marked in **a**

is compressed by compression stress where crack could not nucleate. Besides, the sleeve plunge path in upper sheet is a weak region where crack can easily nucleate and propagate. Figure 12a presents the morphology of fracture surface, in which the upper sheet and lower sheet show different fracture micromorphologies. In upper sheet, the facture surface possesses lots of dimples with nonuniform size, indicating ductile fracture (Fig. 12b). Smooth fracture surface with no obvious dimples is presented at hook (Fig. 12c), which indicates the poor bonding strength. And numerous elongated dimples with coincident size are shown in the fracture surface of lower sheet (Fig. 12d).

Tensile shear fracture in the condition of plunge depth more than 2 mm is shown in Fig. 13. In tensile shear fracture mode, the upward hook leads to stress concentration in hook tip and the SecB between hook and PrimB prevents crack from propagating through the lap interface. Consequently, the crack propagates upward along with SZ/TMAZ interface under tensile stress. Meanwhile, the crack propagates around SZ in upper sheet under compressive stress. Finally, the crack occurs along the orientation of maximum shear stress [32]. As Cao et al. [22] depicted, the results could be explained by the inhomogeneous plastic deformation in the weld leading to strong texture gradients at the SZ/TMAZ interface region. The SEM micrographs of SZ/TMAZ interface are shown in Fig. 14a, which can be divided into two different regions of B and C. Region B exhibits striation direction pattern (Fig. 14b), which reveals that the crack propagates around the weld periphery. Region C is characterized by equiaxed dimples (Fig. 14c), which indicates the good bonding of SZ/TMAZ interface.

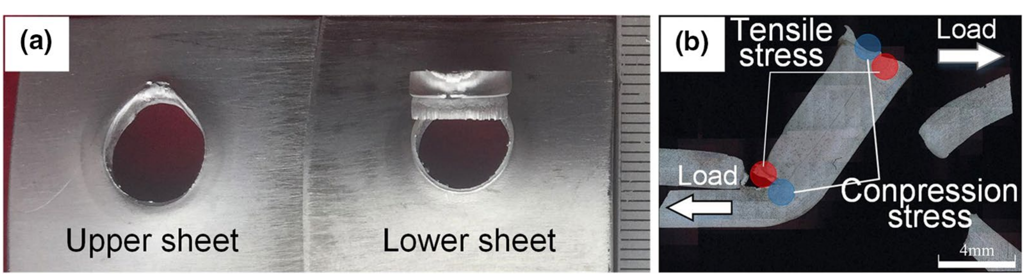

Fig. 11 OM images for plug type facture: **a** macroscopic fracture, **b** cross section

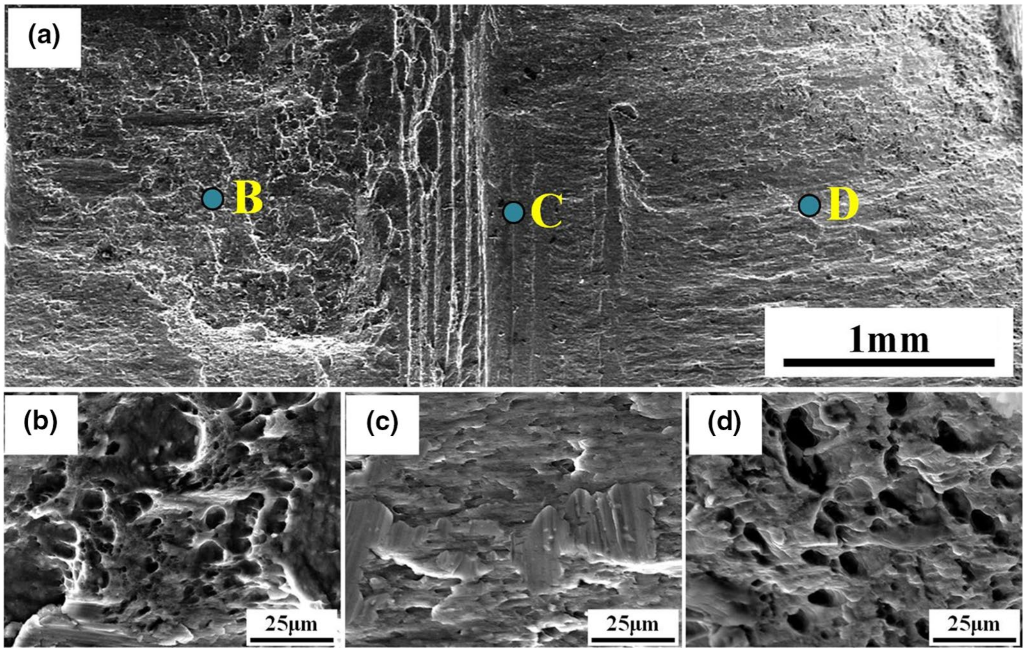

Fig. 12 SEM images of: **a** plug type fracture, **b**–**d** magnified views of the regions B–D marked in **a**

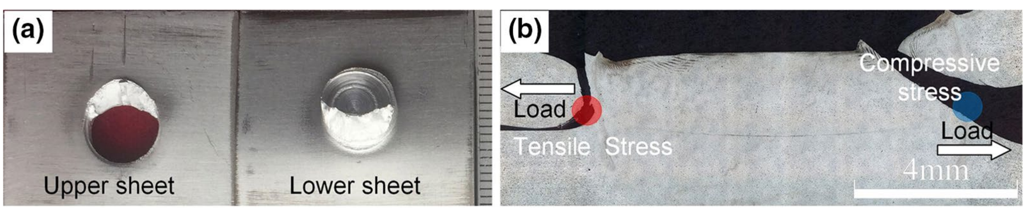

Fig. 13 OM images for tensile shear facture: **a** macroscopic fracture, **b** cross section

4 Conclusions

In the present research, the relationship between sleeve plunge depth, interface characteristics and mechanical properties in 6061-T6 aluminum alloy RFSSWed joint was revealed. The interface characteristics include joint-line remnant and hook, and the joint-line remnant consists of PrimB and SecB. The PrimB shows a poor bonding strength, while SecB shows a good bonding strength. Two types of hook, downward and upward hook, can be observed in joint produced at sleeve plunge depth equal to or greater than 2.0 mm, but no obvious hook is observed in the joint obtained at sleeve plunge depth of 1.75 mm. The height of hook increases with sleeve plunge depth and makes a passive influence to TFSL. The maximum TFSL of 8763.4 N is shown in the joint produced at plunge depth of 2.0 mm. Three types of fracture behaviors of shear, plug and tensile shear fracture are exhibited in joints produced at different plunge depths, which can be ascribed to hook, joint-line remnant and stress distribution during tensile shear test.

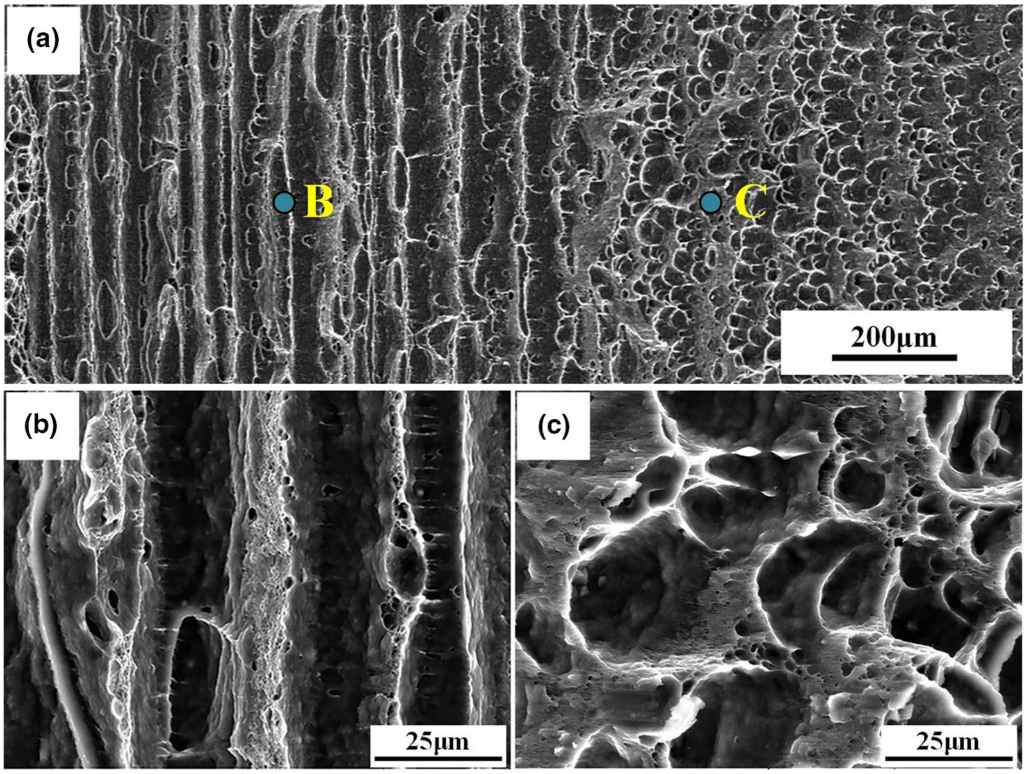

Fig. 14 SEM images of: **a** tensile shear fracture, **b**, **c** magnified views of the regions B and C marked in **a**

Acknowledgements The work was sponsored by the National Science and Technology Major Project (No. 2017ZX04005001), the China Post-doctoral Science Foundation funded project (No. 2015M570287)and the State Key Lab of Advanced Metals and Materials (No. 2017-Z06).

References

[1] L.M. Santana, U.F.H. Suhuddin, M.H. Ölscher, T.R. Strohaecker, J.F.D. Santos, Int. J. Adv. Manuf. Technol. **92**, 4213 (2017)
[2] Y.X. Huang, X.C. Meng, Y.M. Xie, Z.L. Lv, L. Wan, J. Cao, J.C. Feng, Compos. Struct. **189**, 627 (2018)
[3] H. Hameister, An attempt for an industry 4.0 inspired cloud-supported approach for predictive maintenance on the example of refill friction stir spot welding (RFSSW). SAE Tech. Paper (2016). https://doi.org/10.4271/2016-01-2125
[4] Y. Chen, Dissertation, University of Waterloo, 2015
[5] J.A.E. Mazzaferro, T.D.S. Rosendo, C.C.P. Mazzaferro, F.D. Ramos, M.A.D. Tier, T.R. Strohaecker, J.F.D. Santos, Soldag Amp Insp. **14**, 238 (2009)
[6] Z. Xu, Z. Li, S. Ji, L. Zhang, J. Mater. Sci. Technol. **34**, 878 (2018)
[7] M.D. Tier, T.S. Rosendo, J.F.D. Santos, N. Huber, J.A. Mazzaferro, C.P. Mazzaferro, T.R. Strohaecker, J. Mater. Process. Technol. **213**, 997 (2013)
[8] X.W. Yang, T. Fu, W.Y. Li, Adv. Mater. Sci. Eng. **2014**, 1 (2014)
[9] T.Y. Pan, Friction stir spot welding (FSSW)—a literature review. SAE Tech. Paper (2007). https://doi.org/10.4271/2007-01-1702
[10] C. Schilling, J.D. Santos, U.S. patent 6,722,556, 20 April 2004
[11] Y.Q. Zhao, H.J. Liu, Z. Lin, S.X. Chen, J.C. Hou, Sci. Technol. Weld. Join. **19**, 617 (2014)
[12] Y.Q. Zhao, H.J. Liu, Z. Lin, S.X. Chen, J.C. Hou, Mater. Design **62**, 40 (2014)
[13] Z. Shen, X. Yang, S. Yang, Z. Zhang, Y. Yin, Mater. Design **54**, 766 (2014)
[14] M.D. Tier, T.S. Rosendo, J.A. Mazzaferro, C.P. Mazzaferro, J.F.D. Santos, T.R. Strohaecker, Int. J. Adv. Manuf. Technol. **90**, 267 (2017)
[15] H. Badarinarayan, Y. Shi, X. Li, K. Okamoto, Int. J. Mach. Tools Manuf **49**, 814 (2009)
[16] J.Y. Cao, M. Wang, L. Kong, L.J. Guo, J. Mater. Process. Technol. **230**, 254 (2016)
[17] T. Rosendo, M. Tier, J. Mazzaferro, C. Mazzaferro, T.R. Strohaecker, J.F.D. Santos, Fatigue Fract. Eng. Mater. Struct. **38**, 1443 (2015)
[18] J.J. Shen, S.B.M. Lage, U.F.H. Suhuddin, C. Bolfarini, J.F.D. Santos, Metall. Mater. Trans. A **49**, 1 (2018)
[19] Z. Shen, X. Yang, Z. Zhang, L. Cui, Y. Yin, Mater. Design **49**, 181 (2013)
[20] Y.M. Yue, Y. Shi, S.D. Ji, Y. Wang, Z.W. Li, J. Mater. Eng. Perform. **26**, 5064 (2017)
[21] L. Zhou, L.Y. Luo, T.P. Zhang, W.X. He, Y.X. Huang, J.C. Feng, Int. J. Adv. Manuf. Technol. **92**, 3425 (2017)
[22] J.Y. Cao, M. Wang, L. Kong, H.X. Zhao, P. Chai, Mater. Charact. **128**, 54 (2017)
[23] M. Reimann, J. Goebel, J.F.D. Santos, Mater. Des. **132**, 283 (2017)
[24] P.L. Li, Z.F. Xu, C. Yu, H. Lu, J.S. Yao, G.Y. Chen, Acta Metall. Sin. (Engl. Lett.) **25**, 225 (2012)
[25] Y. Zhao, H. Liu, T. Yang, Z. Lin, Y. Hu, Int. J. Adv. Manuf. Technol. **83**, 1467 (2016)
[26] P. Su, A. Gerlich, T.H. North, G.J. Bendzsak, Sci. Technol. Weld. Join. **11**, 163 (2006)

[27] S. Venukumar, S. Yalagi, S. Muthukumaran, T. Nonferr, Metal. Soc. **23**, 2833 (2013)
[28] S. Ji, Y. Wang, J. Zhang, Z. Li, Int. J. Adv. Manuf. Technol. **90**, 1 (2016)
[29] Z. Li, S. Gao, S. Ji, Y. Yue, P. Chai, J. Mater. Eng. Perform. **25**, 1673 (2016)
[30] Z. Shen, X. Yang, Z. Zhang, L. Cui, T. Li, Mater. Design **44**, 476 (2013)
[31] A. Kubit, M. Bucior, D. Wydrzyński, T. Trzepieciński, M. Pytel, Int. J. Adv. Manuf. Technol. **94**, 4479 (2018)
[32] Z. Li, S. Ji, Y. Ma, P. Chai, Y. Yue, S. Gao, Int. J. Adv. Manuf. Technol. **86**, 1925 (2016)